Chemical Physics Letters 482 (2009) 143–147

Contents lists available at ScienceDirect

Chemical Physics Letters

journal homepage: www.elsevier.com/locate/cplett

Dynamics of vibrational and electronic coherences in the electronic excited state studied in a negative-time range

Takayoshi Kobayashi [a,b,c,d,*], Atsushi Yabushita [c]

[a] ICORP, JST, 4-1-8 Honcho, Kawaguchi, Saitama 332-0012, Japan
[b] Department of Applied Physics and Chemistry and Institute for Laser Science, University of Electro-Communications, 1-5-1 Chofugaoka, Chofu, Tokyo 182-8585, Japan
[c] Department of Electrophysics, National Chiao-Tung University, Hsichu 300, Taiwan
[d] Institute of Laser Engineering, Osaka University, 2-6 Yamada-oka, Suita, Osaka 565-0971, Japan

ARTICLE INFO

Article history:
Received 19 March 2009
In final form 6 October 2009
Available online 9 October 2009

ABSTRACT

Femtosecond pump–probe spectroscopy signals in a negative-time range (i.e., when the probe pulse precedes pump pulse) were analyzed to study the dynamics of electronic and vibrational coherences in the photodissociation of oxyhemoglobin. The decay time of the electronic coherence between the ground and Q-band electronic states is found to be 45 ± 5 fs. The dephasing times of the vibrational modes of several frequencies in the ground state have been determined. Those in the excited state are found to be ~26 fs. The absence or presence of the modes in the negative-time range due to the excited state wavepacket is explained in terms of the mode coupling strength.

1. Introduction

The structures of heme proteins have been studied by many research groups for several decades because of their critical importance in oxygen transfer in biological systems [1–7]. Previous studies have demonstrated that hemoglobin (Hb), heme proteins, and heme model systems have similar heme photophysics [8–13]. All of these hemes have two intermediates, designated Hb_I^* and Hb_{II}^*. Experiments have revealed that Hb_I^* is formed within 50 fs and subsequently decays to form Hb_{II}^* within 300 fs. The Hb_{II}^* electronic state has a lifetime of ~3 ps and it decays to the ground state.

Very detailed studies have been conducted to explain the results obtained by Champion's group for myoglobin and its ligated species. From experimental analysis, they concluded that the observed spectral change can be explained simply by the temperature increase in the sample [14,15]. Previous studies had investigated photodissociation at wavelengths shorter than 500 nm. By contrast, the present study investigates photodissociation in the visible spectral region between 520 and 720 nm.

Models that assume either the generation of short-lived intermediate(s) or a temperature increase can potentially describe the ultrafast dynamics observed in the visible spectral region. In the discussion of the ultrafast dynamics observed in the present study, we tentatively follow the former model, which assumes that two intermediates are formed.

In a previous study, we found that Hb_I^* was formed at 45 ± 5 fs after the excitation of oxyhemoglobin. We also found that both the photodissociation and the out-of-plane motion of the heme iron occur very rapidly (<50 fs) to create a species that resembles deoxy Hb. Hb_I^* transient spectra appeared on the same time scale as photolysis in both Hb^* CO and Hb^* NO [13].

In the present Letter, we have performed ultrafast pump–probe spectroscopy for a negative-time range as well as a positive time range. The analysis for vibrational modes in both of the two time ranges has allowed us to clearly distinguish the dynamics of excited state from that of ground state. We have thus determined the vibrational dephasing time of modes coupled to the transition between in the relevant electronic states.

2. Experimental

Hemoglobin from bovine blood (Sigma–Aldrich) was dissolved in water with a phosphate buffer stabilized at pH 7.7. Undissolved residue was removed by passing the solution through a filter (Millex; Millipore) inserted over the head of a syringe. To prevent oxidization of the sample, sodium thiosulfate (Tokyo Chemical Industry, Ltd.) was added to the solution without further purification. The sample solution had an optical density of ~1.0 at 540 nm in a 1-mm cell (6210-27501; GL Science) used for femtosecond pump–probe experiments. The solutions were carefully prepared while monitoring their absorption spectra using an ultraviolet–visible–near-infrared scanning spectrophotometer (UV-3101PC; Shimadzu).

A Ti:sapphire laser system (FemtoSource (sPRO); FemtoLasers) with an eight-path bow-tie amplifier (Femtopower; FemtoLasers)

* Corresponding author. Address: Department of Applied Physics and Chemistry and Institute for Laser Science, University of Electro-Communications, 1-5-1 Chofugaoka, Chofu, Tokyo 182-8585, Japan. Fax: +81 42 443 5845.
E-mail address: kobayashi@ils.uec.ac.jp (T. Kobayashi).

0009-2614/$ - see front matter © 2009 Elsevier B.V. All rights reserved.
doi:10.1016/j.cplett.2009.10.013

was used as the light source in the pump–probe experiments. The pulses generated by the amplifier had a width of 20 fs, an energy of 30 μJ, a spectral range of 750–870 nm, and a repetition rate of 1 kHz. The output pulse was frequency-doubled using a type-I β-barium borate (BBO) crystal and compressed using a prism pair to generate a 395 nm pulse having a width of 40 fs at a repetition rate of 1 kHz. The frequency-doubled pulse was used as the pump pulse in the pump–probe measurements.

After generating the frequency-doubled pulse in the BBO crystal, a portion of the fundamental (i.e., non-frequency-doubled) pulse remains in the light path of the pump beam. One of the prisms used for compressing the pump beam displaced the residual fundamental pulse, which was compressed to 20 fs by passing through another prism pair. The compressed fundamental pulse was focused on a sapphire plate to generate a visible broadband spectrum by causing self-phase modulation in the sapphire plate. This visible broadband pulse was used as the probe pulse in the pump–probe measurements.

Both the pump and probe pulses were focused by a parabolic mirror into a 1-mm-thick standard fluorimeter cell (6210-27501; GL Science). The time delay of the probe pulse relative to the pump pulse was varied using an electrical stepper with a 1-fs step. The pump–probe signals were detected using a 128-channel lock-in amplifier. All measurements were performed at room temperature (294 ± 1 K).

The observed stationary spectrum of the sample has peaks at 540, 573, and 624 nm. The peak locations agree with those given in Ref. [16]. The laser pulse spectrum extends from 520 to 720 nm with a peak around 570 nm with a good overlap with the stationary absorption spectrum of the sample.

3. Results and discussion

3.1. Delay time-dependence of difference absorbance and time-resolved difference absorption spectra

Fig. 1 shows the laser spectrum and the absorption spectrum of the oxyhemoglobin solution sample. There is a very good overlap between the laser spectrum and the sample absorption. The laser spectrum consists of a main peak at 17 500 cm^{-1}, a weak peak around 14 500 cm^{-1}, and a shoulder at ~16 000 cm^{-1}. The absorption spectrum has two clearly separated peaks around 18 550 and 17 300 cm^{-1}, which are assigned to $Q(00)$ and $Q(10)$, respectively.

Fig. 2a shows the probe delay time dependence of the absorbance change probed at 556, 588, 617, 653, and 685 nm in the observation time range from −70 to 1900 fs. The sample is first excited to the S_2 state (the Soret band of heme) by the 395-nm pump pulse. The positive signal of the absorbance change observed in the visible region of Fig. 2a is probably the excited state absorption from the S_2 state to a higher-lying excited state. Fig. 2b shows Fourier power spectra of the time trace from 50 to 430 fs. In Ref. [17], we classified the dynamic vibronic couplings in vibrational real-time spectra. Discussion on the probe wavelength dependence of the Fourier power spectra is left to a future study after the vibrational phases of molecular vibrations have been observed at a higher signal-to-noise ratio.

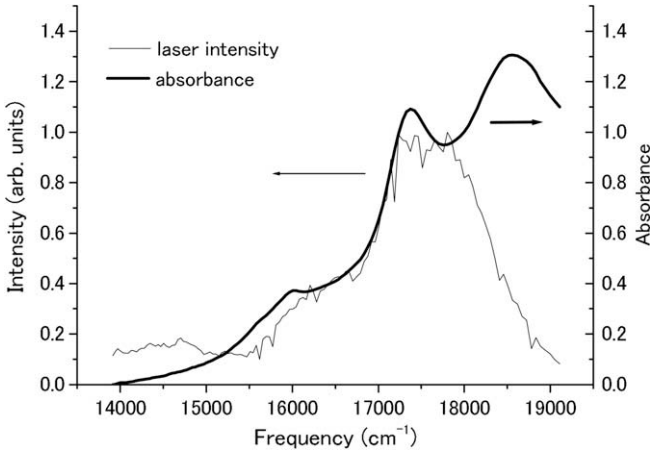

Fig. 1. Laser spectrum (thin line) and absorption spectrum of oxyhemoglobin solution sample (thick line).

Petrich et al. [13] performed time-resolved absorption measurements of hemoglobin, myoglobin, and protoheme for both ligated and unligated diatomic molecules. The spectral range was in the near UV and blue region between 400 and 490 nm. They observed the absorbance change for HbO_2 at 414 nm and found that it could be described by

$$\Delta A(t) = \Delta A'_1 \exp\left(\frac{-t}{\tau'_1}\right) + \Delta A'_2 \exp\left(\frac{-t}{\tau'_2}\right) + \Delta A'_3 \exp\left(\frac{-t}{\tau'_3}\right) + \Delta A'_4 \exp\left(\frac{-t}{\tau'_4}\right), \quad (1)$$

where the time constants τ'_1, τ'_2, τ'_3, and τ'_4 were determined to be <50 fs, 300 fs, 2.5 ps, and ≫10 ps, respectively.

We performed oxyhemoglobin pump–probe measurements using ultrashort pulses and determined the spectra of $\Delta A'_1$, $\Delta A'_2$, $\Delta A'_3$, and $\Delta A'_4$ from the data between 583 and 719 nm. The time constants obtained in the present study are considered to correspond to those obtained in Ref. [13] in the following manner: $\tau_1 = \tau'_1$, τ_1 is obtained from a mixed contribution of the components of τ'_2 and τ'_3, and τ_3 is the remaining part. The present measurement up to 1.9 ps does not permit us to measure the time constant of 2.5 ps due to the mixture of τ'_2 and τ'_3. Though the probe wavelength region in the present study differs from that of Ref. [13], good agreement between the time constants obtained in both studies implies that the same dynamics are observed in these cases.

3.2. The time-dependent difference absorbance in the negative-time range

Several unexpected finite-size signals, which appear to violate causality, are observed in the real-time traces observed over the entire range of probe photon energies. The signal intensities decrease as the delay time becomes increasingly negative and they almost completely disappear at a delay time of about −70 fs. Near time zero, there are several spiky signals that have relatively high intensities and whose temporal profiles vary periodically between a dispersive shape and an absorption or emission shape on changing the probe photon energy (wavelength). There are oscillatory structures for positive delay times (i.e., when the pump pulse precedes the probe pulse).

The density matrix equations for the two-level system were solved to second order in the pump field and to first order in the probe field. This provides the simplest solution from which the basic physical mechanisms can be readily understood.

The differential spectrum of the probe transmittance was found to consist of three distinct components. The first is proportional to the level population changes induced by the pump and that are present when the probe arrives. This level population term gives a signal characteristic of the spectral hole-burning experiments in which coherent effects do not play an important role. It is the only term that persists when the probe follows the pump and it decays with time constant T_1.

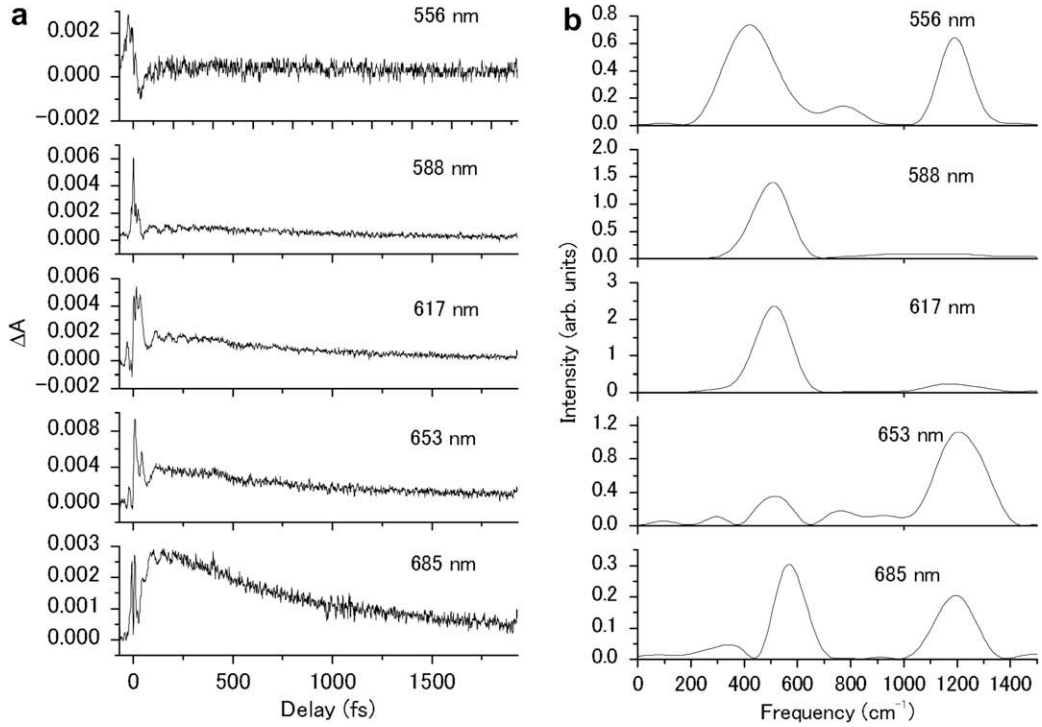

Fig. 2. (a) Several real-time traces of difference absorbance at 556, 588, 617, 653, and 685 nm for probe delay times from −70 to 1930 fs. (b) Fourier power spectra of real-time traces from 50 to 430 fs.

The second component is proportional to the pump-induced polarization present when the probe arrives. The probe field interacts with this pump-induced polarization to create a spatial modulation of the level populations. The pump field then interacts with this population modulation to create a polarization component that is spatially coherent with the probe; this is referred to as the pump polarization coupling term. This second component is effective only when the pump pulse overlaps with the probe pulse, as it requires the presence of the pump both before and after the probe arrives.

The third and final component is proportional to the unperturbed population differences and occurs because the pump field modifies the otherwise free decay of the probe-induced polarization. We refer to this term as the perturbed free-induction decay term. It persists when the probe precedes the pump and rises with a time constant T_2. It also continues to be relatively important when the pump is detuned from the molecular resonance, so that the level populations are unaffected and the pump-induced polarization is relatively small. In this case, it can be considered to be a result of the pump-induced dynamic Stark shift of the molecular resonance. The signal in the negative-time range is discussed below in terms of the perturbed free-induction decay.

Fig. 3a shows a coherent artifact generated by the buffer solution stored in the 1-mm-thick glass cell. The signal was averaged over the probe wavelength from 573 to 586 nm (i.e., near the peak of the probe spectrum) where the coherent artifact was observed with a high intensity. It demonstrates that the artifact can modify the shape of time traces between −10 and 10 fs.

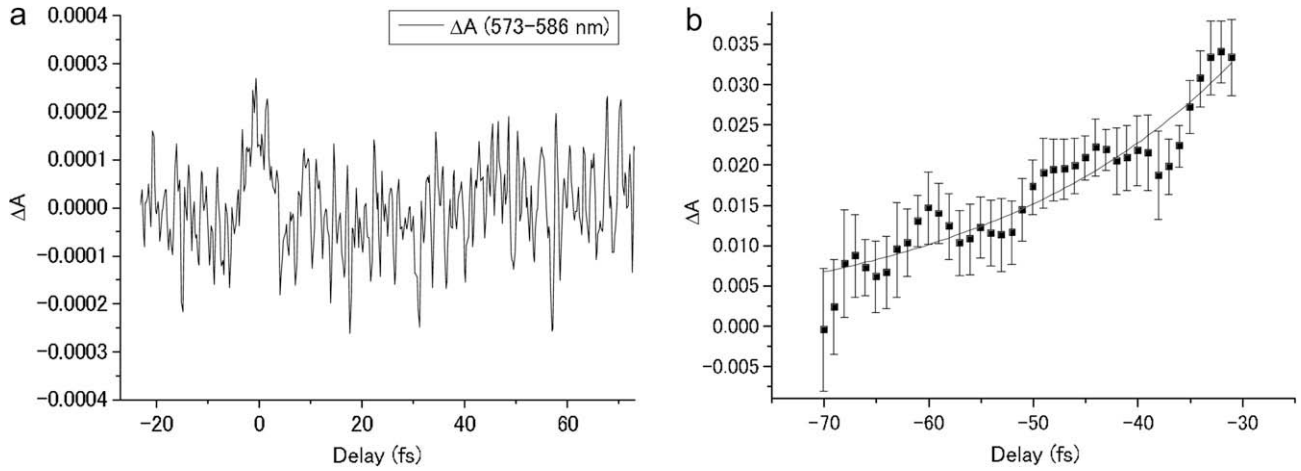

Fig. 3. (a) Coherent artifact generated by the buffer solution stored in a 1-mm-thick glass cell. The signal was averaged over the probe wavelengths from 573 to 586 nm. (b) Real-time trace (thin curve) of absorbance change integrated over the spectral range from 552 to 571 nm and a single exponential function (thick curve) fitted in the negative delay time region.

Fig. 3b shows a real-time trace of the absorbance change integrated over the spectral range from 552 to 571 nm and a single exponential fitted decay function in the negative delay time region. The time trace grows exponentially from −70 to −30 fs. However, it starts to be greatly modulated after −30 fs, reflecting the high vibrational coherence around a delay of zero. This modulation makes it difficult to perform an exponential fit. Therefore, we used the data from −70 to −30 fs for the exponential fit in Fig. 3b. The analysis gave an electronic dephasing time of $T_2 = 25 \pm 2$ fs from the plot shown in Fig. 3b. The dephasing rate $1/T_2$ obtained from the plots consists of the following three components

$$\frac{1}{T_2} = \frac{1}{2T_1} + \frac{1}{T_2'} + \frac{1}{T_2^*}. \tag{2}$$

Here, T_1 is the population decay time, and T_2' and T_2^* are the pure electronic dephasing time and the phase relaxation time due to inhomogeneous broadening, respectively. The short population decay time $T_1 = \tau_1 = 45$ fs of the excited state lifetime, which corresponds to the formation of Hb_I^* after the excitation of oxyhemoglobin, was determined from real-time traces for positive delay times, as described in the foregoing. Then, from $T_2 = 25 \pm 2$ fs and $T_1 = \tau_1 = 45$ fs, $(1/T_2' + 1/T_2^*)^{-1} = 34.6$ fs is obtained.

Therefore, the lower limit of the two time constants, T_2' and T_2^*, is 34.6 fs. To discuss the absolute value of the pure phase relaxation time constant T_2', we require information on T_2^*. However, since it is difficult to determine its value, the discussion here is based on the lower limit of its value.

As shown in Fig. 1, the absorption spectrum has two clearly separated peaks around 18 550 and 17 300 cm^{-1}, which are attributed to $Q(00)$ and $Q(10)$, respectively. The inhomogeneous broadening is expected to be small enough to resolve the two vibrational peaks. This indicates that the phase relaxation time is substantially longer than the molecular vibrational period of 26.7 fs, which corresponds to a frequency of 1250 cm^{-1} of the vibrational structure. Therefore, together with the lower limit value of 34.6 fs, $T - 2^*$ can safely be assumed to be considerably longer than the period, and T_2' is determined to be ~35 fs. Thus, ~72% of the phase decay is due to pure dephasing and ~28% is due to population decay associated with the electronic relaxation due to the extremely fast photodissociation. Such a short, pure dephasing time may indicate that the preceding ultrafast photodissociation occurs in the electronic coherence of the electronic excited state of the hemoglobin molecule. It can also be concluded that the inhomogeneity has a relatively small effect, and it is estimated to be less than ~10% of the width broadening due to the total electronic phase relaxation.

Fig. 4 shows the Fourier power spectra of the oscillating components of the real-time traces in a positive time range (50 to 700 fs) and a negative-time range (−70 to −10 fs). The mean real-time trace in the probe wavelength region between 653 and 673 nm was used for the Fourier analysis to enhance the signal-to-noise ratio. The power spectra are quite different; the peak frequencies of the components of the spectra are summarized in Table 1. The power spectrum in the positive time range has five prominent peaks at 210, 393, 554, 731, and 1106 cm^{-1}, whose lifetimes were determined to be 449, 366, 555, 1085, and >1300 fs, respectively. The power spectrum in the negative-time range has a peak with a peak frequency of about 1255 cm^{-1}. The real-time trace in the negative-time range is pertinent to the wavepacket motion on the potential surface of the excited state. The interaction scheme that is responsible for the oscillatory feature in the negative-time region is described in Refs. [18,19]. The dephasing time of the mode was found to be 26 fs from the bandwidth. The molecular configuration changes after photodissociation due to the breaking of the O_2-heme porphyrin bond. When the mode associated with photodissociation (i.e., the Fe–O_2 stretching mode) is not coupled

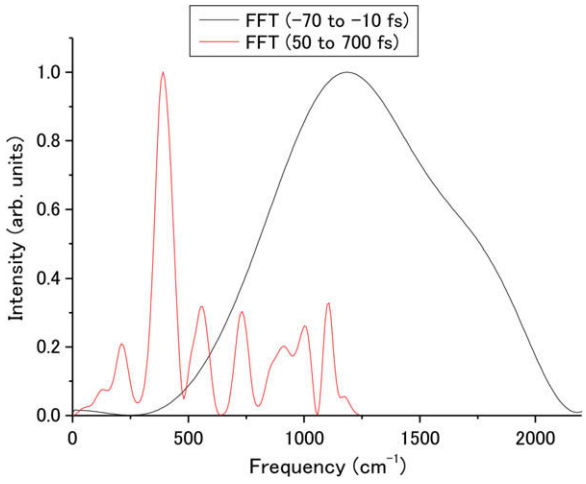

Fig. 4. Fourier power spectra of the oscillating component in the negative-time range (−70 to −10 fs, black curve) and the positive time range (50 to 700 fs, red curve) of the mean time trace over the probe wavelength region from 652 to 673 nm. (For interpretation of the references to colour in this figure legend, the reader is referred to the web version of this article.)

Table 1
Peak frequencies of the Fourier power spectra of the oscillating components of the real-time traces in the positive and negative-time ranges.

	Frequency (cm^{-1})	Width (cm^{-1})	Lifetime (fs)	Assignment
Negative-time range	1254	782	26	δ (C_mH)
	210	69	449	ν (Fe–His)
	393	74	336	δ (C–CH_3)
Positive time range	554	65	555	ν (Fe–O_2)
	731	57	1085	ν (pyr breathing)
	1106	44	>1300	ν ($C_β$-methyl)

to other specific modes, the frequencies of these modes are not greatly affected by the dissociation. Of the modes listed in Table 1 with mode assignments, the modes with frequencies of 210, 393, 554, and 731 cm^{-1} do not appear in the negative-time range. From the mode characteristics, these modes are thought to couple with the Fe–O_2 stretching mode so that they are strongly affected by the dissociation, resulting in rapid dephasing, which is why they are absent in the negative-time range. The peaks observed in the negative delay region are assigned to excited state wavepacket motions because of their short lifetimes. Since the peak frequencies observed for positive delays differ from those observed for negative delays, which is assigned to excited state dynamics, the peaks in the positive delay region are assigned to the ground state wavepacket.

4. Conclusion

Utilizing data in the negative-time range of ultrafast pump–probe spectroscopy (i.e., when the probe pulse precedes the pump pulse), we have studied the dynamics of electronic coherence between the excited electronic and ground states and that of vibrational coherence in the electronic excited state. The dephasing time of the electronic coherence consisting of a linear combination of the ground state and the Q-band electronic state is found to be 45 ± 5 fs. The vibrational dephasing times of modes with frequencies of 210, 393, 554, 731, and 1106 cm^{-1} are found to be 449, 366, 555, 1085, and >1330 fs, respectively. The dephasing time of the vibrational mode with a frequency of 1255 cm^{-1} is found to be 26 fs. The absence or presence of modes in the negative-time

range due to the excited state wavepacket is explained in terms of the mode coupling strength.

Acknowledgments

This research was supported in part by a Grant-in-Aid for Specially Promoted Research (No. 14002003), the program for the Promotion of Leading Researches in Special Coordination Funds for Promoting Science and Technology from the Ministry of Education, Culture, Sports, Science and Technology (MEXT) of Japan. This work was also supported in part by the ICORP program of Japan Science and Technology Agency (JST), a grant to A.Y. from the National Science Council of the Republic of China, Taiwan (NSC 98-2112-M-009-001-MY3), and a grant from the Ministry of Education (MOE) under the Aim for the Top University and Elite Research Center Development Plan (ATU Plan) in National Chiao-Tung University (NCTU).

References

[1] M.F. Perutz, W. Bolton, R. Diamond, H. Muirhead, H.C. Watson, Nature 203 (1964) 687.
[2] H. Muirhead, J. Cox, L. Mazzarella, M.F. Perutz, J. Chim. Phys. 65 (1968) 188.
[3] S. Franzen, B. Bohn, C. Poyart, G. Depillis, S.G. Boxer, J.L. Martin, J. Biol. Chem. 270 (1995) 1718.
[4] D.G. Lambright, S. Balasubramanian, S.G. Boxer, Chem. Phys. 158 (1991) 249.
[5] S. Franzen, S.G. Boxer, J. Biol. Chem. 272 (1997) 9655.
[6] S. Franzen, J.C. Lambry, B. Bohn, C. Poyart, J.L. Martin, Nature Struct. Biol. 1 (1994) 230.
[7] E.H. Harutyunyan et al., J. Mol. Biol. 251 (1995) 104.
[8] J.M. Baldwin, C. Chothia, J. Mol. Biol. 129 (1979) 175.
[9] S. Franzen, B. Bohn, C. Poyart, G. DePillis, S.G. Boxer, J.L. Martin, J. Biol. Chem. 270 (1995) 1718.
[10] S. Franzen, B. Bohn, C. Poyart, J.L. Martin, Biochemistry 34 (1995) 1224.
[11] J.L. Martin, A. Migus, C. Poyart, Y. Lecarpentier, R. Astier, A. Antonetti, Proc. Natl. Acad. Sci. USA 80 (1983) 173.
[12] M.F. Perutz, Ann. Rev. Biochem. 48 (1979) 327.
[13] J.W. Petrich, C. Poyart, J.L. Martin, Biochemistry 27 (1988) 4049.
[14] X. Ye et al., J. Phys. Chem. 107 (2003) 8156.
[15] X. Ye, A. Demidov, P.M. Champion, J. Am. Chem. Soc. 124 (2002) 5914.
[16] R.R. Anderson, A. Parrish, J. Invest. Dermatol. 77 (1981) 13.
[17] T. Kobayashi, Z. Wang, T. Otsubo, J. Phys. Chem. A. 111 (2007) 12985.
[18] B. Cruz, J.P. Gordon, P.C. Becher, C.V. Shank, IEEE J. Quant. Electron. 24 (1988) 261.
[19] T. Kobayashi, J. Du, W. Feng, K. Yoshino, Phys. Rev. Lett. 101 (2008) 037402.